Simple and complex square waves in an edge-emitting diode laser with polarization-rotated optical feedback

Athanasios Gavrielides*
Air Force Research Laboratory AFRL/EOARD, 86 Blenheim Crescent, Ruislip Middlesex HA4 7HB, United Kingdom

David W. Sukow,† Guinevere Burner, Taylor McLachlan, John Miller, and Jake Amonette
Department of Physics and Engineering, Washington and Lee University, 204 W. Washington St., Lexington, Virginia 24450, USA
(Received 5 January 2010; published 19 May 2010)

Numerical and experimental results are presented for an edge-emitting diode laser with delayed optical feedback, where the polarization state of the feedback is rotated such that the natural laser mode is coupled into the orthogonal, unsupported mode. We examine the bifurcation structure and dynamics that give rise to a class of periodic, polarization-modulated solutions, the simplest of which is a square wave solution with a period related to but longer than twice the external cavity roundtrip time. Such solutions typically emerge when the feedback is strong and the differential losses in the normally unsupported polarization mode are small. We also observe more complex waveforms that maintain the same periodicity.

DOI: 10.1103/PhysRevE.81.056209 PACS number(s): 05.45.Xt, 42.55.Px, 42.65.Pc, 42.60.Mi

I. INTRODUCTION

Optical feedback from an external reflector is a well-known mechanism for inducing dynamical effects in semiconductor lasers. The behavior that results depends on many factors, such as the laser architecture and operating conditions, the external cavity length and configuration, and the strength of the feedback. One particular case of interest is where the polarization state of the optical feedback is made to be orthogonal to the laser's natural operating mode.

Such systems are of interest from a variety of standpoints, and their nonlinear dynamical properties have been investigated [1–6]. They exhibit the typical features of general delay-dynamical systems, and thus can exhibit behavior similar to that found in time-delay systems from diverse fields. Indeed, square waveforms such as we present in this paper are well-known in the Mackey-Glass model [7], which has wide applications in biology, or Ikeda's equation [8,9], which can be interpreted a bistable optical device. Other studies consider the relationship between rotated optical feedback and optoelectronic feedback systems, in which the laser field couples directly to the carriers via electrical means [6,10].

Special attention has been given to rotated optical feedback with vertical-cavity surface-emitting lasers (VCSELs), in which the feedback gives rise to mode-locking [11,12] and to switching between the dominant polarization mode and the orthogonal mode that is nearly degenerate due to the cylindrical symmetry of such devices [13–20]. Such polarization self-modulation has a variety of useful applications stemming from the production of optical pulses at multi-giga-Hertz repetition rates without the need for high-speed electronics [21]. Edge-emitting lasers can also be made to exhibit pulse trains generated by polarization self-modulation, even though the losses in the orthogonal mode are typically higher than in VCSELs [22–26]. This previous work has typically employed a quarter-wave plate as the polarization-rotating element, which allows mutual coupling between the polarization modes as well as multiple cavity roundtrips due to reflections from the laser's front facet.

In this paper, we consider edge-emitting, Fabry-Pérot laser diodes with feedback that couples only the natural, horizontal polarization mode to the unsupported, orthogonal mode. This configuration has the advantages of eliminating multiple-roundtrip reflections. It also simplifies the analysis since the orthogonal mode, even when activated by feedback, cannot influence the natural mode directly via optical injection. In other words, there is unidirectional coupling from the natural polarization to the orthogonal one. Studies of the fundamental dynamics of this system [27–30], as well as its chaos synchronization properties [31–33], demonstrate the need for both polarization modes to be considered to capture the full behavior of this system.

In previous work, we showed that this system produces polarization self-modulated square waves, and that such behavior arises analytically from the model as a bifurcation phenomenon [34]. Therefore, our purpose in this paper is to present results that explore further the origins and variations of these dynamical phenomena. We first elucidate the bifurcation structure of this system, using a two-polarization model in numerical studies, which demonstrates the emergence of square-wave solutions from limit cycles at low feedback. Then, we present experimental observations of polarization self-modulated waves, confirming simple square waves but emphasizing the more complex forms with the same periodicity that include both square and pulsating elements. The mathematical model and numerical findings are presented in the next section, followed by experimental observations afterward.

II. MATHEMATICAL MODEL

The model we use to examine square wave solutions is the full two polarization model in which the horizontal natu-

*tom.gavrielides@london.af.mil
†sukowd@wlu.edu

ral polarization is delayed, rotated to the vertical polarization and then reinjected into the semiconductor laser [27,28]. We do not require any terms for multiple external cavity roundtrip reflections, because our cavity configuration extinguishes them. By design, emission in the vertical mode does not affect the natural mode directly, instead acting through the carriers. The two complex fields E_1 and E_2 and the carriers N thus are expressed as

$$\frac{dE_1}{dt} = (1 + i\alpha)NE_1, \tag{1}$$

$$\frac{dE_2}{dt} = (1 + i\alpha)(N - \beta)E_2 + \eta e^{-i(\omega_1\tau + \phi_e)}E_1(t - \tau), \tag{2}$$

$$T\frac{dN}{dt} = P - N - (1 + 2N)[|E_1|^2 + |E_2|^2]. \tag{3}$$

The first equation describes the horizontal polarization that lases naturally since it has the lowest losses. The second equation describes the vertical polarization with β the additional loss that this polarization experiences. The last term in this equation describes the reinjection of the rotated horizontal polarization after a time delay τ, the cavity roundtrip time. Finally, the last equation describes the inversion of the carriers with which both polarization fields interact. The phase factor $e^{-i(\omega_1\tau+\phi_e)}$ corresponds to a phase due to the propagation in the external cavity and it includes any additional constant phase due to transmission or reflection from optical elements that may be present in the cavity. This term can be absorbed totally in the redefinition of $E_1(t)$, and therefore it does not affect the dynamics and will be eliminated from any further considerations. The three complex equations have been expressed in dimensionless quantities with the time normalized to the cavity lifetime of the diode laser. The α parameter corresponds to the linewidth enhancement factor and the quantity T is equal to the ratio of the carriers lifetime to the cavity lifetime. P is the pumping above threshold of the diode laser and η, a real quantity, is the strength of the feedback of the polarization rotated field.

The range of parameters for which the square wave emerges appears to be fairly broad and it requires that the differential losses be small. The rest of the quantities are assumed to be representative of a SDL semiconductor laser [35]. We have fixed $T=150$, and $\alpha=2$. The differential loss is set to $\beta=0.03$ and the pumping level to $P=0.5$. We have examined a large range of normalized delays from $\tau=100$ to as large as $\tau=10000$ and we have found essentially the same behavior. In fact, as the length of the external cavity becomes longer the square wave behavior dominates for smaller values of feedback.

For our computations we have normalized the time to the relaxation frequency $s=\omega t$, a small number defined by $\omega = \sqrt{2P/T}$, and redefined the inversion to $N=\omega Z$. With these definitions we obtain

$$\frac{dE_1}{ds} = (1 + i\alpha)ZE_1, \tag{4}$$

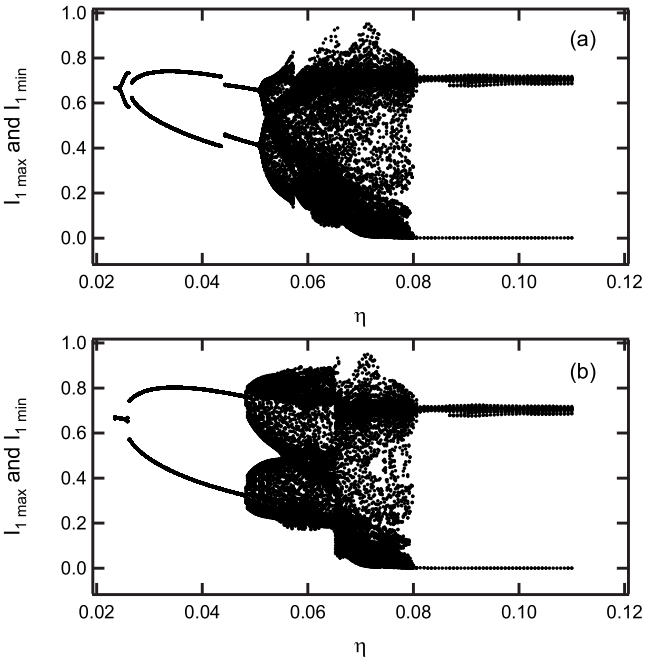

FIG. 1. Bifurcation diagrams of maxima and minima of the intensity of the two polarizations I_1, I_2 as a function of feedback. (a) shows a set of four coexisting attractors, and (b) shows the development of the limit cycle that emerges from the steady state. The parameters used are $P=0.5$, $T=150$, $\alpha=2$, and $\tau=1000$.

$$\frac{dE_2}{ds} = (1 + i\alpha)(Z - \beta\omega^{-1})E_2 + \eta\omega^{-1}E_1(s - \vartheta), \tag{5}$$

$$\frac{dZ}{ds} = \frac{1}{2P}[P - \omega Z - (1 + 2\omega Z)(|E_1|^2 + |E_2|^2)]. \tag{6}$$

where $\vartheta=\omega\tau$. In terms of amplitude-phase decomposition $E_i=A_i e^{i\phi_i}$ we obtain:

$$\frac{dA_1}{ds} = ZA_1, \tag{7}$$

$$\frac{dA_2}{ds} = (Z - \beta\omega^{-1})A_2 + \eta\omega^{-1}A_1(s - \vartheta)\cos(\Psi), \tag{8}$$

$$\frac{d\Psi}{ds} = \alpha[Z(s - \vartheta) - Z + \beta\omega^{-1}] - \eta\omega^{-1}\frac{A_1(s - \vartheta)}{A_2}\sin(\Psi), \tag{9}$$

$$\frac{dZ}{ds} = \frac{1}{2P}[P - \omega Z - (1 + 2\omega Z)(|E_1|^2 + |E_2|^2)], \tag{10}$$

where $\Psi=\phi_1(s-\vartheta)-\phi_2$.

Bifurcation diagrams for the parameters of the previous paragraphs are shown in Fig. 1 with an external delay of $\tau=1000$, which corresponds in the calculations to a normalized external cavity delay $\theta=81.65$. In Fig. 1(a) at least four different attractors are shown, and they can be identified by the discontinuous breaks as a function of the feedback strength. There is a limit cycle that emerges at weak feed-

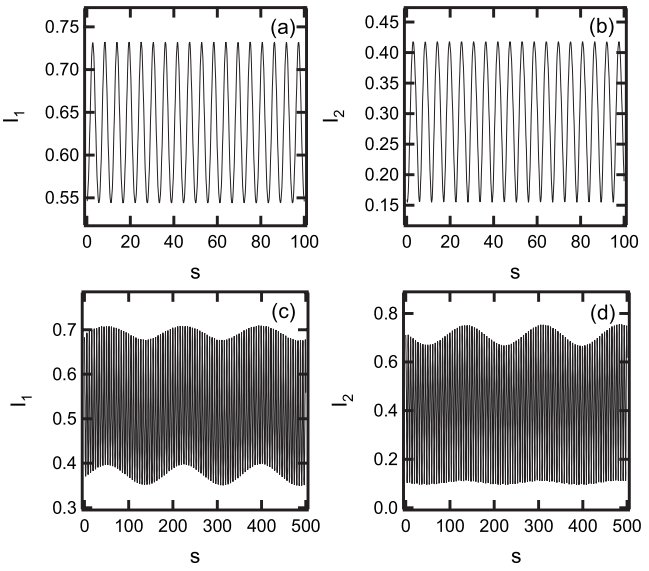

FIG. 2. (a) and (b) show the limit cycles of the two polarization I_1, and I_2, for η=0.03 and (c) and (d) show the modulation of the limit cycles by a second frequency at η=0.049. Parameters used are the same as in the caption of Fig. 1.

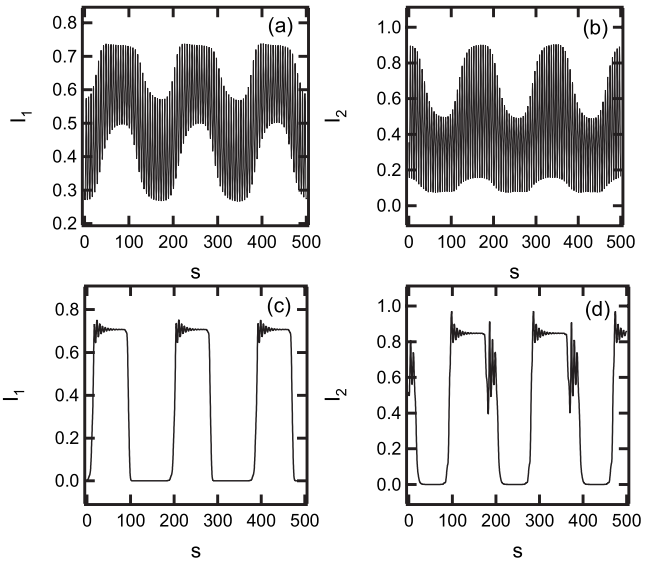

FIG. 3. (a) and (b) show waveforms of a two frequency torus at η=0.05, and (c) and (d) square waveform for the intensity of the two polarizations at η=0.32. Parameters are the same as in the caption of Fig. 2.

back from the steady state and two limit cycles that emerge from periodic limit points. All three have the same frequency that is close to the relaxation frequency, and their development into their respective attractors is not followed in this particular bifurcation diagram. The third limit cycle, however, is followed into its own chaotic attractor. At large feedback this chaotic attractor develops into the square wave that is discussed in the next few paragraphs. In Fig. 1(b) the limit cycle that emerges from the steady state is followed for all of its development and into the square wave. Contrasting Figs. 1(a) and 1(b) one notices that the attractors at η=0.05 are different and it is obvious that at least two coexisting attractors exist. However, the bifurcation diagram in Figs. 1(a) and 1(b) for $\eta \geq 0.065$ shows that the dynamics remain on a single attractor. At significantly higher η than appear on this diagram, multiple attractors coexist for simple and complex square waveform solutions; experimental data of several such waveforms will be shown later in this paper.

The sequence of bifurcations that leads to the square wave behavior is related to the Hopf bifurcation from which an in-phase oscillation at the relaxation frequency for the two polarizations of the system are born. Indeed, for all of the limit cycles at low feedback the oscillations are in phase for both polarizations. In Figs. 2(a) and 2(b), we show the limit cycle of the intensity of both polarizations $I_1=|E_1|^2$ (horizontal) and $I_2=|E_2|^2$ (vertical) at the feedback of η=0.03. For stronger feedback η=0.049, a second frequency is introduced and modulates the limit cycle of the intensity of the two polarizations but out of phase as shown in Figs. 2(c) and 2(d). The period of this new frequency is related to the external cavity round trip time and it is about 10%–15% larger than twice the external cavity time. As the feedback is further increased to η=0.05, this modulation becomes stronger and deeper with an envelope that becomes more and more in nature close to a square waveform as shown in Figs. 3(a) and 3(b). In addition, the relaxation oscillations are retained but diminished in amplitude. Eventually the waveforms become totally square keeping the out of phase relationship, retaining a few small and decaying amplitude oscillations at the relaxation frequency as shown in Figs. 3(c) and 3(d) at a feedback of η=0.32. Experimental spectral evidence of relaxation oscillation and torus solutions in the weak-feedback regime is recorded in Ref. [6]. However, no smooth transition from a torus solution to fully developed square waves has been observed experimentally, due primarily to the multistability of the system.

We have found several waveforms that are still in nature square as in Figs. 3(c) and 3(d) but they can become progressively more and more complicated. They usually show such behavior in short cavities and dominate much of the dynamics. They still retain their relationship to the period of the external cavity round trip and do not show any further development into chaos as the feedback is increased. One such waveform is shown in Fig. 4 in the which the two polarizations are plotted as a function of normalized time. The pa-

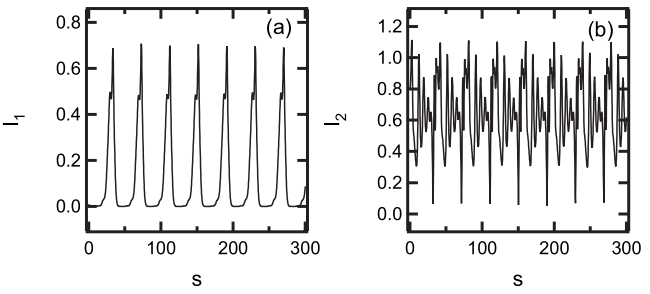

FIG. 4. (a) and (b) show a more complicated square waveform that retains still its periodic behavior. All parameters are the same as in the caption of Fig. 2 except that τ=100.0 and the feedback is η=0.42.

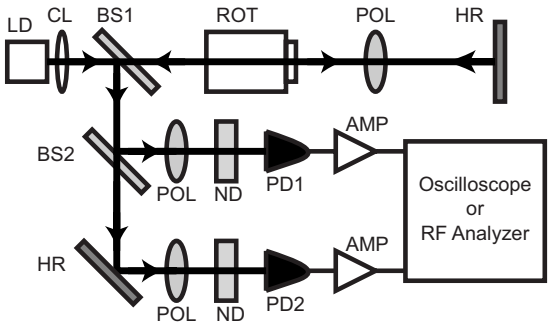

FIG. 5. Schematic diagram of experimental apparatus.

rameters used for these calculations are the same as in the bifurcation diagrams except the external cavity round trip time is reduced to $\tau=100$, and the feedback is set to $\eta=0.42$.

III. EXPERIMENT

The experimental apparatus is illustrated schematically in Fig. 5. The laser under study is a SDL-5401 laser diode (LD), an index-guided Fabry-Pérot multiple quantum well (MQW) device that is stabilized in temperature to ± 0.01 K. It has an operating wavelength $\lambda=817.9$ nm and current threshold of 18.48 mA. The feedback system is a linear external cavity that includes elements to rotate the polarization of the feedback and to control its strength. After the laser beam emerges from a collimating lens (CL), it passes through a nonpolarizing plate beam splitter (BS1) that transmits 70% of the incident beam. It continues through a Faraday rotator (ROT), which is simply a Faraday isolator with its input polarizer removed and output polarizer oriented 45° from horizontal. After emerging from the rotator now polarized at 45°, it encounters a rotatable linear polarizer (POL) used for attenuation, and is retroreflected from a highly reflective mirror (HR). The reflected beam passes unchanged through the polarizer and re-enters the Faraday rotator through its input polarizer, assuring its 45° polarization orientation. The beam rotates an additional 45° to vertical and is thus reinjected into the laser in an orthogonal polarization relative to its natural output mode. We note that this configuration prevents feedback from multiple roundtrips, since any vertically polarized light reflected from the laser facet back into the cavity will be extinguished by the Faraday's output polarizer.

Polarization-resolved detection is accomplished via the signal reflected from BS1. The reflected beam (30% of the incident ray) strikes a second nonpolarizing beam splitter (BS2) with R=50%. The two resulting beams enter similar detection arms, consisting of POL configured to pass either the horizontal or vertical signals, and neutral density filters (ND) to limit the power incident on the photodetectors (PD1 and PD2). The ac signals from these 8.75 GHz detectors (Hamamatsu C4258–01) are amplified by 23 dB using wideband (10 kHz–12 GHz) amplifiers (AMP), and are captured and analyzed by use of either a digital storage oscilloscope (LeCroy 8600, 6 GHz analog bandwidth) or a microwave spectrum analyzer (Agilent E4405B).

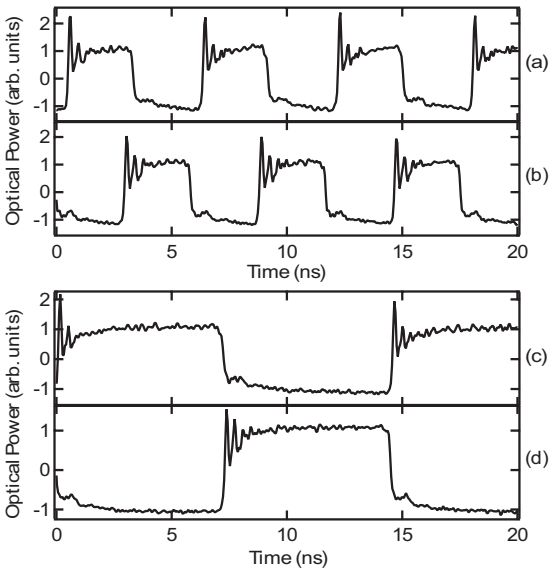

FIG. 6. Experimental time series of square waves. Graphs (a) and (b) show horizontal and vertical modes, respectively, when $\tau=2.60$ ns. In graphs (c) and (d) $\tau=6.92$ ns.

With this experimental system, we observe the square wave solutions that are predicted numerically, as well as more complex periodic waveforms. Two pairs of square waves are illustrated in Fig. 6, as were reported previously [34]. Graph in Fig. 6(a) shows the horizontal polarization mode and Fig. 6(b) the simultaneous vertical mode, when the external cavity length is $L=39$ cm, leading to a roundtrip time $2L/c=2.60$ ns. The pump current is set at 28.02 mA and the roundtrip power transmission in the cavity is 37.6%. A clean square wave with damped oscillations is evident, very similar to Fig. 3. The horizontal and vertical modes are out of phase. The waves have a period of 5.85 ns, slightly longer than two cavity roundtrips (by 0.65 ns), which is consistent with numerical findings and observations reported in Ref. [28]. Observations with dc-coupled detectors indicate the waves are fully modulated, consistent with numerical results shown in Figs. 3(c) and 3(d).

To further demonstrate that these solutions have periods near $4L/c$, Figs. 6(c) and 6(d) show the horizontal and vertical modes when the external cavity length is increased to 104 cm. The period has increased correspondingly to 14.50 ns, and relaxation oscillations continue to be apparent when the wave switches polarization.

Another view of these signals is provided in the frequency domain. Figure 7 shows the RF power spectra of the time series shown in Fig. 6, with graphs in Figs. 7(a) and 7(b) corresponding to the same experimental conditions as in Figs. 6(a) and 6(b), respectively The first peak appears at 170 MHz, the fundamental frequency of the square wave, followed predominantly by the odd harmonics as expected from classical Fourier theory. The first even harmonic is initially over 30 dB lower than the fundamental.

In addition to pure square waves, we also have found complex solutions with square-wave periods near $4L/c$, similar to the numerical observations of complex waves displayed in Fig. 4. These are often a combination of square and

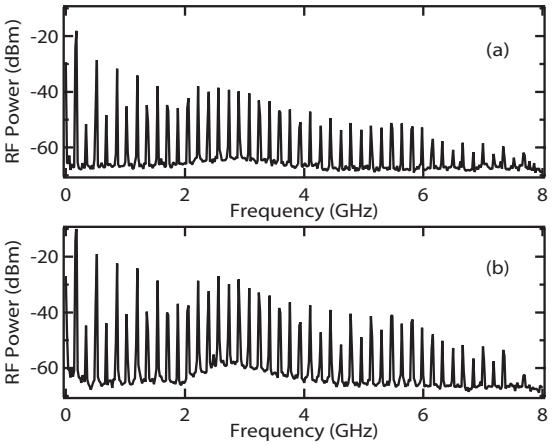

FIG. 7. Experimental RF spectra of square waves. Graphs (a) and (b) show power spectra of horizontal and vertical modes, respectively, when $\tau=2.60$ ns.

pulsating forms, and we devote the remainder of this section to illustrating their properties. First, we note that the antiphase relationship between polarization modes still persists for the complex $4L/c$ forms. Experimental time series of one such solution are shown in Fig. 8. Graphs in Figs. 8(a) and 8(b) show the horizontal and vertical polarization modes, respectively. For these data, the pump current remains at 28.02 mA and the roundtrip power transmission in the cavity is 37.6%. The external cavity length is returned to $L=39$ cm so $2L/c=2.60$ ns. The period once again is 5.85 ns, and although the waves now include short pulses as well as square features, the clear antiphase relationship between polarization components persists. This solution, as well as several other complex square waveforms, coexist with the simple square wave shown in Fig. 6.

Figure 9 shows the radio frequency (RF) power spectra of the time series data illustrated in Fig. 8. Graphs in Figs. 9(a) and 9(b) correspond to Figs. 8(a) and 8(b), respectively, showing the RF spectra of both polarization modes. The fundamental peak in both spectra is again at 170 MHz, confirming the $4L/c$ periodicity, but the structure differs subtly from the pure square wave, and includes greater frequency content at higher harmonics due to the pulsations.

To further examine the relationship between pulsations and square waves, it is helpful to increase the external cavity

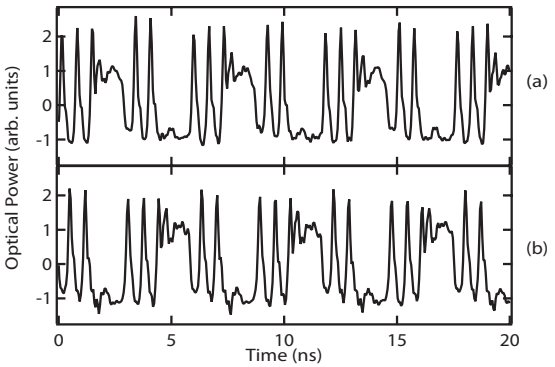

FIG. 8. Experimental time series of complex waves.

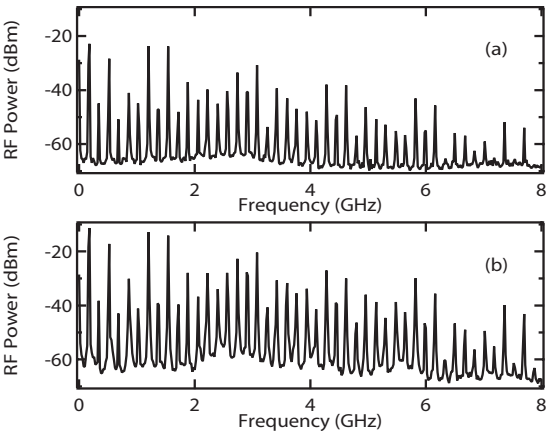

FIG. 9. Experimental RF spectra of complex waves.

length and thus $4L/c$, and to adjust other parameters: $L=59$ cm, $\tau=2L/c=3.93$ ns, and pump current is 36.0 mA. A sequence of time series recorded under these conditions is shown in Fig. 10. For visual clarity, only horizontal polarizations are shown in this figure, but we have verified that the antiphase relationship between horizontal and vertical modes still exists as demonstrated in Fig. 8. The sequence of waves from Figs. 10(a)–10(d) is shown in order of decreasing feedback, with external cavity roundtrip transmissions of 44.4%, 36.4%, 27.5%, and 22.0%, respectively. However, while increasing numbers of pulsations tend to appear as the feedback is decreased, many of these solutions actually coexist simultaneously with one another under a given set of operating conditions. Coexisting solutions are a frequently observed feature of complex, delay-differential systems, and this aspect of the dynamics will be discussed elsewhere. Another important feature of these results is that the strongly pulsating behavior can be observed independently or combined with the $4L/c$ periodicity, and this subject will be examined further in the next figure.

The polarization-rotated optical feedback system is known to produce a wide variety of dynamical states, includ-

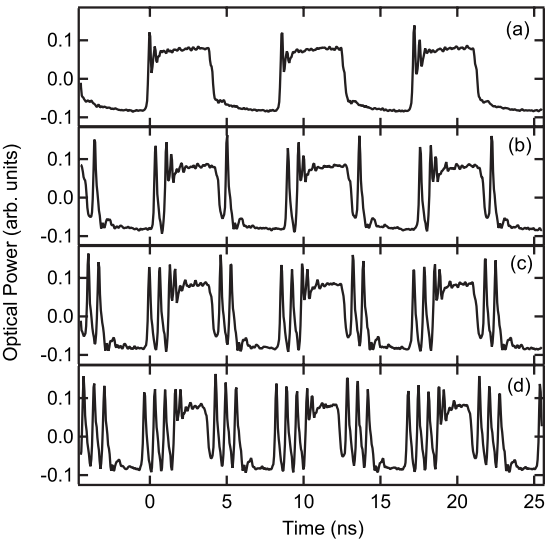

FIG. 10. Experimental time series of complex waves with $4L/c$ periodicity.

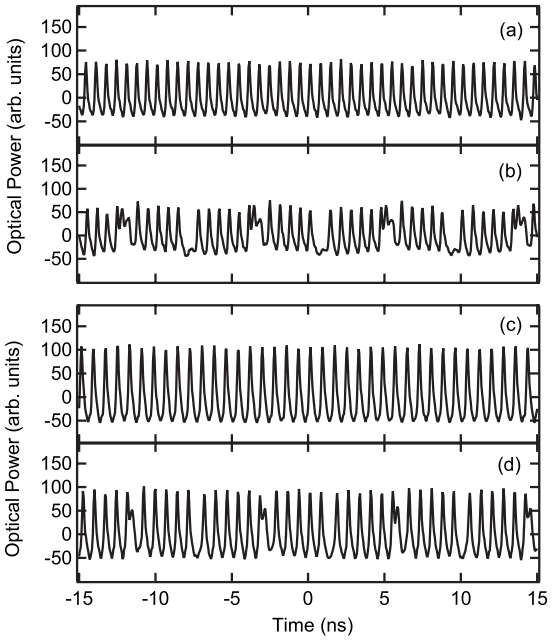

FIG. 11. Experimental time series showing related pulsating and $4L/c$ states.

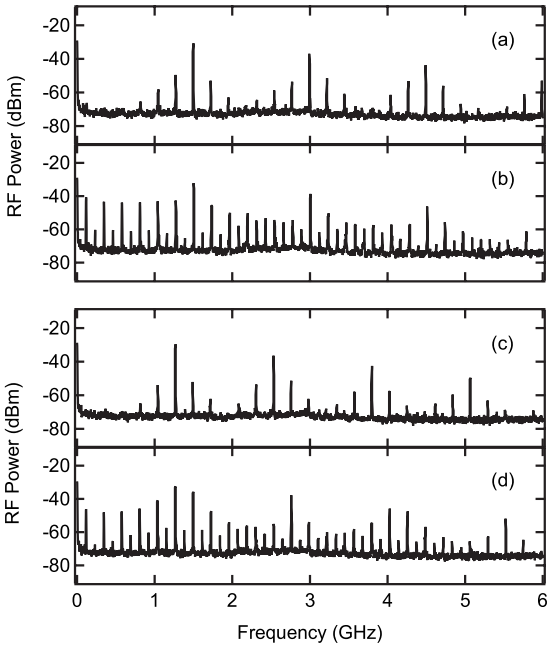

FIG. 12. Experimental RF spectra showing related pulsating and $4L/c$ states.

ing quasiperiodic, chaotic, and strongly pulsating solutions. Figure 11 illustrates in the time domain how pulsating states can be related to square wave $4L/c$ states; frequency domain measurements will follow in Fig. 12. To make these measurements, a small modification of the experimental apparatus is made, by substituting a 5% reflective beamsampler in place of the 30% plate beamsplitter (element BS1 in Fig. 5). This increases the maximum possible cavity roundtrip transmission. The experimental parameters for Fig. 11 are otherwise the same as in Fig. 10, and again only a single polarization is shown for clarity.

Figure 11(a) illustrates a strongly pulsating state when the external cavity roundtrip transmission is 45.1%. The pulsations are strong and regular, with a period of 0.665 ns, or frequency of 1.504 GHz. In Fig. 11(b), a $4L/c$ periodicity is overlaid upon the pulsating state, while the pulsation period remains the same. The roundtrip transmission is decreased to 26.0% in Fig. 11(b). When the feedback range is changed, we observe the same phenomenon occurring with a different pulsation period. In Fig. 11(c), the roundtrip transmission is 79.2% and a larger but slower pulsating state is present. When the feedback is decreased to 63.9% in Fig. 11(d), the squarewave periodicity once again is present. Again, multiple coexisting solutions are present at these feedback levels, so the cavity transmissions stated are representative only and not to be interpreted as unique.

RF spectral representations of the same data are shown in Fig. 12. Graphs in Figs. 12(a)–12(d) correspond directly to the data shown in Figs. 11(a)–11(d), respectively. Figure 12(a) shows a set of combs in the frequency domain, characteristic of pulsations, with a peak frequency at 1.504 GHz and sidebands located with spacing of $c/2L$. In Fig. 12(b), the strongest peak remains at 1.504 GHz but now the low-frequency square wave signature is also present. The same phenomena appear in Figs. 12(c) and 12(d), but with the pulsation frequency now decreased to 1.266 GHz, which is very close to $c/2L$ less than 1.504 GHz with $L=59$ cm.

IV. SUMMARY

In summary, we have studied the two-polarization model for an edge-emitting semiconductor laser with delayed, polarization-rotated optical feedback. The feedback unidirectionally couples the natural, horizontal polarization to the vertical mode which is normally suppressed. We find that the model of this system predicts periodic square-wave solutions, along with a variety of complex solutions whose periods are associated with twice the external cavity roundtrip time. Such solutions are observed numerically and experimentally, under conditions where the differential losses are small. Experimental observations also show that the system can exhibit multiple coexisting solutions, including complex waveforms with $4L/c$ periodicity that also include pulsations.

ACKNOWLEDGMENT

This material is based upon work supported by the U.S. National Science Foundation under CAREER Grant No. 0239413.

[1] K. Otsuka and J.-K. Chern, Opt. Lett. **16**, 1759 (1991).
[2] T. C. Yen, J. W. Chang, J. M. Lin, and R. J. Chen, Opt. Commun. **150**, 158 (1998).
[3] J. Houlihan, G. Huyet, and J. G. McInerney, Opt. Commun. **199**, 175 (2001).
[4] F. Rogister, A. Locquet, D. Pieroux, M. Sciamanna, O. Deparis, P. Megret, and M. Blondel, Opt. Lett. **26**, 1486 (2001).
[5] F. Rogister, D. Pieroux, M. Sciamanna, P. Megret, and M. Blondel, Opt. Commun. **207**, 295 (2002).
[6] J. M. Saucedo Solorio, D. W. Sukow, D. R. Hicks, and A. Gavrielides, Opt. Commun. **214**, 327 (2002).
[7] M. C. Mackey and L. Glass, Science **197**, 287 (1977).
[8] K. Ikeda, K. Kondo, and O. Akimoto, Phys. Rev. Lett. **49**, 1467 (1982).
[9] M. Nizette, Phys. Rev. E **70**, 056204 (2004).
[10] P. Saboureau, J.-P. Foing, and P. Schanne, IEEE J. Quantum Electron. **33**, 1582 (1997).
[11] J. Javaloyes, J. Mulet, and S. Balle, Phys. Rev. Lett. **97**, 163902 (2006).
[12] J. Mulet, J. Javaloyes, and S. Balle, IEEE J. Quantum Electron. **43**, 786 (2007).
[13] H. Li, A. Hohl, A. Gavrielides, H. Hou, and K. Choquette, Appl. Phys. Lett. **72**, 2355 (1998).
[14] F. Robert, P. Besnard, M. L. Charles, and G. M. Stephan, IEEE J. Quantum Electron. **33**, 2231 (1997).
[15] J. Martin-Regalado, F. Prati, M. San Miguel, and N. B. Abraham, IEEE J. Quantum Electron. **33**, 765 (1997).
[16] G. Ropars, P. Langot, M. Brunel, M. Vallet, F. Bretenaker, A. Le Floch, and K. D. Choquette, Appl. Phys. Lett. **70**, 2661 (1997).
[17] M. Giudici, S. Balle, T. Ackemann, S. Barland, and J. R. Tredicce, J. Opt. Soc. Am. B **16**, 2114 (1999).
[18] M. Sciamanna, F. Rogister, O. Deparis, P. Megret, M. Blondel, and T. Erneux, Opt. Lett. **27**, 261 (2002).
[19] M. Sciamanna, T. Erneux, F. Rogister, O. Deparis, P. Megret, and M. Blondel, Phys. Rev. A **65**, 041801(R) (2002).
[20] J. Mulet, M. Giudici, J. Javaloyes, and S. Balle, Phys. Rev. A **76**, 043801 (2007).
[21] J.-L. Cheng and T.-S. Yen, Opt. Commun. **271**, 503 (2007).
[22] C. L. Tang, J. Opt. B: Quantum Semiclassical Opt. **10**, R51 (1998).
[23] W. H. Loh, Y. Ozeki, and C. L. Tang, Appl. Phys. Lett. **56**, 2613 (1990).
[24] W. H. Loh and C. L. Tang, Opt. Commun. **85**, 283 (1991).
[25] W. H. Loh, C. L. Tang, and L. Chung, IEEE J. Quantum Electron. **27**, 389 (1991).
[26] W. H. Loh, A. T. Schremer, and C. L. Tang, IEEE Photon. Technol. Lett. **2**, 467 (1990).
[27] T. Heil, A. Uchida, P. Davis, and T. Aida, Phys. Rev. A **68**, 033811 (2003).
[28] D. W. Sukow, A. Gavrielides, T. Erneux, M. J. Baracco, Z. A. Parmenter, and K. L. Blackburn, Proc. SPIE **5722**, 256 (2005).
[29] M. Oriá, B. Farias, T. Sorrentino, and M. Chevrollier, J. Opt. Soc. Am. B **24**, 1867 (2007).
[30] L. Khaykovich, T. Galfsky, Z. Shotan, and N. Gross, Opt. Commun. **282**, 2059 (2009).
[31] D. W. Sukow, A. Gavrielides, T. Erneux, M. J. Baracco, Z. A. Parmenter, and K. L. Blackburn, Phys. Rev. A **72**, 043818 (2005).
[32] N. Shibasaki, A. Uchida, S. Yoshimori, and P. Davis, IEEE J. Quantum Electron. **42**, 342 (2006).
[33] Y. Takeuchi, R. Shogenji, and J. Ohtsubo, Appl. Phys. Lett. **93**, 181105 (2008).
[34] A. Gavrielides, T. Erneux, D. W. Sukow, G. Burner, T. McLachlan, J. Miller, and J. Amonette, Opt. Lett. **31**, 2006 (2006).
[35] T. B. Simpson and J. M. Liu, J. Appl. Phys. **73**, 2587 (1993); J.-M. Liu and T. B. Simpson, IEEE J. Quantum Electron. **30**, 957 (1994).